Formalized Drawing of Fullerene Nets. 2. Applications to Mapping of Pyracylene Rearrangements, C_2-Insertion/Elimination Pathways, and Leapfrog/Carbon Cylinder Operations

Mitsuho Yoshida and Eiji Ōsawa*

Computational Chemistry Group, Department of Knowledge-Based Information Engineering, Toyohashi University of Technology, Tempaku-cho, Toyohashi, Aichi 441

(Received March 23, 1995)

The net drawing method of fullerenes presented in the preceding paper has been applied to the predictive studies on the movements of pentagonal rings accompanying skeletal transformations in fullerenes. The products of pyracylene rearrangements have been systematically generated to examine low-energy isomers containing abutting pentagons (so-called anti-IPR isomers) by performing the rearrangement only once on all the pyracylene units in each of the C_{60} to C_{100} isomers. The Endo-Kroto mechanism of C_2-insertion into the carbon framework of fullerene has been likewise shown to be executable on paper. In this way, several energetically favorable pathways of growth have been found for C_{76} to C_{90}. Potential applications of net drawing to the leapfrog and carbon cylinder operations and C_2-elimination are also mentioned.

In the preceding paper,[1] we have presented a new algorithm for the formalized drawing of net diagrams of fullerenes on equilateral triangular lattice. Our method is based on a historical design of icosahedron net by Dürer[2] and consists of dividing a fullerene structure into two caps and a tubular segment. One of the caps, containing six pentagonal rings, is placed on top of the other cap, containing the rest six pentagons, while the tubular segment is placed between the caps. This formalism allows anyone to draw fullerene nets in a systematic way and to read out the characteristics of the fullerene structure with ease, especially the spatial distribution of pentagonal rings.

In addition to its ability of exhaustively generating isomeric fullerene structures as demonstrated in the preceding paper,[1] our drawing method presents a novel means to study skeletal transformations of fullerenes on paper: Invariant and variant portions of the transforming structure can be readily distinguished on the net. We illustrate below how the pyracylene rearrangement pathways[3] and the growth mechanisms through incorporation of C_2 fragments[4] can be systematically treated. The leapfrog[5] and carbon cylinder[6] operations, novel methods of producing fullerenes having favorable HMO configurations, can be conveniently handled as well.

Pyracylene Rearrangements on the Net Diagram

The pyracylene rearrangement generally refers to a locally degenerate isomerization on the molecular surface of fullerene involving rotation of the central CC bond in a *pyracylene unit* by a right angle (Scheme 1). The rearrangement has been proposed by Stone and Wales in an early study of non-soccer ball structures for C_{60}.[3] Although such an isomerization has not been detected experimentally, the isolated isomers of C_{78}[7,8] and C_{84}[9] are shown to be the most stable structures in the trajectories of pyracylene rearrangement sequences. This rearrangement is considered essential in separating abutted pentagonal rings during the formation of fullerenes,[10] a process called annealing.[11] Recent finding of a low-energy mechanism for the pyracylene rearrangement by Scuseria[11] involving changes in hybridization adds strength to the above view. Since the pyracylene rearrangement is basically a migration of pentagonal rings over the molecular surface of fullerene, we explore below a convenient way of describing the migration on the net.

A pyracylene unit appears in a fullerene net when two corners (pentagonal rings) are separated by $\sqrt{3}$ on the equilateral triangular lattice. It is convenient to distin-

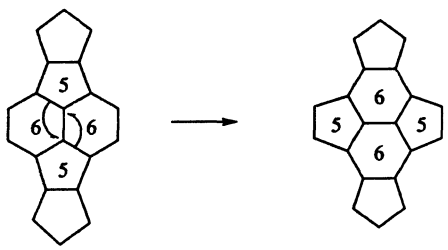

Scheme 1.

guish three types of corner configuration: along the edge of a cap (type A, Fig. 1a), at the base of a cap (type B) or across the tubular segment (type C). For simplicity, the unit is symbolized by a thick bar connecting the pair of corners as shown in Fig. 1. The type A, wherein the unit is cut open, is symbolized by shaded edges. The pyracylene rearrangement can be achieved on the diagram by appropriately displacing corners, which can be graphically represented by rotation and translation of the bar or the shaded edges as illustrated in Fig. 1b, followed by adjustments in the vicinity. The adjustments differ depending on the types A to C, as illustrated in Fig. 2.

A small program PYRA[12] was written to perform the rearrangement as well as the accompanying adjustments automatically. The program receives the triangular coordinates of corners (namely the structure of a fullerene), rearranges all the pyracylene units one by one and outputs the changed coordinates of the products, which are then processed with program FULLER[1,12] to identify the structure. There is no need to treat adjacency matrices or Cartesian coordinates when the structural changes due to the migration of five-membered rings are pursued on a net diagram.

We first checked the IPR-to-IPR pyracylene rearrangement pathways for C_{60} to C_{100}. The results of enumeration are summarized in Table 1. Compared to the exponential increase in the number of isomers with the number of carbon atoms,[13] the number of Stone–Wales isomerization paths is small in the range of fullerenes examined: There are only 11 such isomerization pathways for C_{100}. The results agree with those of Fowler and his group,[10] who covered these paths by a symmetry-based search on the ring spiral codes.

1. Generation of Anti-IPR Isomers. A recent suggestion on the presence of isomeric C_{60} in

Table 1. Number of Pyracylene Rearrangement Pathways (p) in IPR Fullerenes C_n (n=60 to 100)

n	p	n	p	n	p
60	0[a]	80	1	92	5
70	0	82	1	94	5
72	0	84	2	96	7
74	0	86	1	98	8
76	0	88	2	100	11
78	1	90	3		

a) Degenerate paths are ignored.

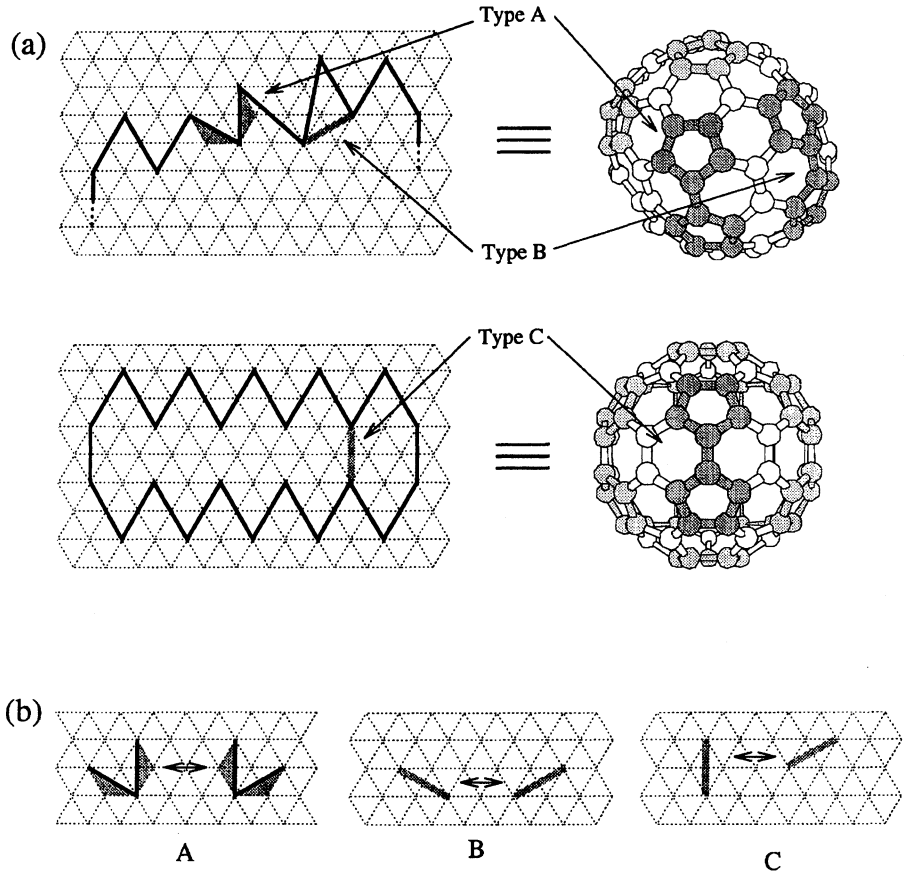

Fig. 1. (a) Pyracylene units (dark shaded) at the tip of a cap (A), at the base of a cap (B), and across the tubular segment (C). In the corresponding perspective drawing of fullerene on the right, pentagons involved in the rearrangement are dark shaded. (b) Scheme of basic operations to be applied to the pyracylene unit to effect the rearrangement types A to C.

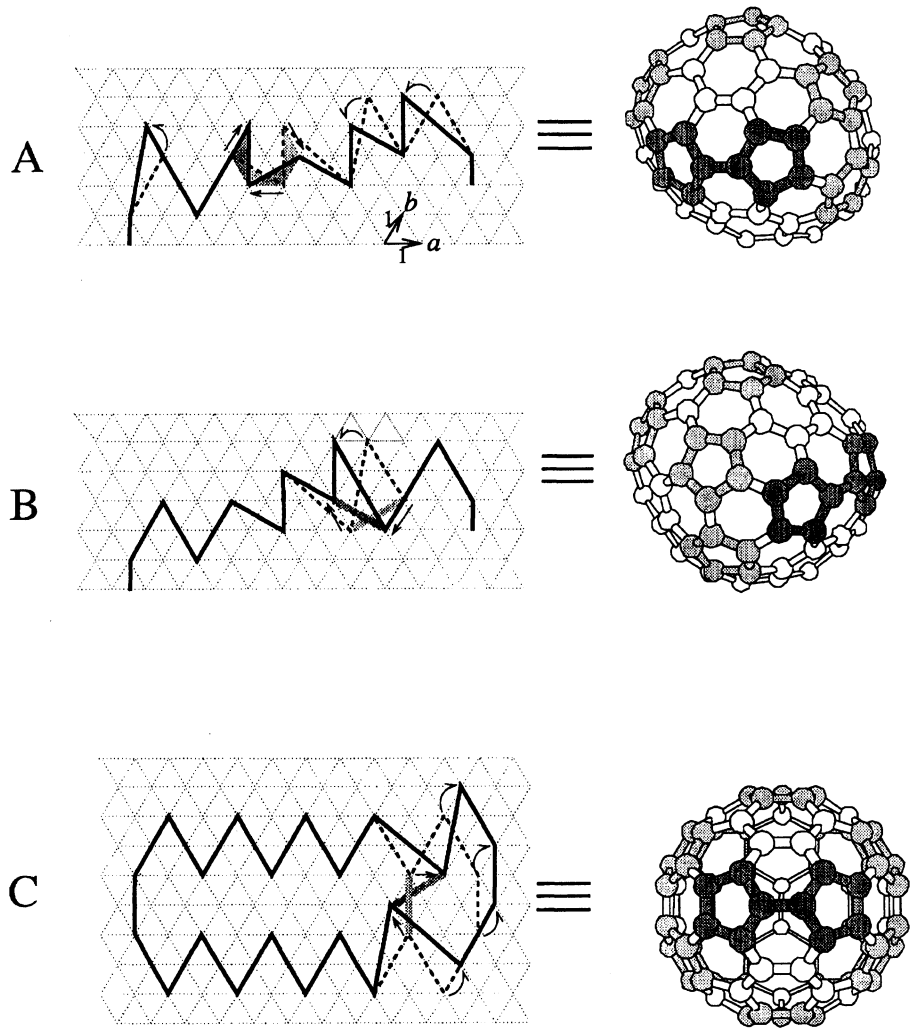

Fig. 2. Net diagrams before (dotted line) and after (solid line) the pyracylene rearrangement. Perspective drawings on the right represent the rearranged structure, which should be compared with starting structures shown in Fig. 1a. (A) The rotation-translation of pyracylene unit is followed by successive rotation of the rest of *tip* corners in the same cap by 60° about the *base* corners. Despite the seemingly extensive changes in the diagrams, only the two V_5s in the pyracylene unit are actually relocated as can be visualized by the perspective drawing of fullerenes on the right. A lattice point on a triangular coordinates is denoted by (m,n), where m and n means displacements from an origin (0,0) along the base directions (a,b), respectively. A rotation of this point by ±60° around an origin into a new position (m',n'), is expressed by the following integer operations on a triangular lattice: $m'=-n$, $n'=m+n$ for 60° rotation and $m'=m+n$, $n'=-m$ for −60° rotation. (B) Only one tip corner needs to be adjusted after rotating the unit, in this case to satisfy the closing condition of the cap. (C) All the corners to the right of the rearranged pyracylene unit must be adjusted as shown. Tubule vector changes only in this case by ±1 along base axis in the course of rearrangement.

the soot from benzene flame[14] has aroused interests in the stability of fullerene isomers containing abutting pentagons.[15] Especially interesting in this respect are the higher fullerenes up to C_{100}, for which isolation work is well in progress[16] and which might be able to accommodate some anti-IPR isomers due to the decreasing strain in the carbon framework. The problem with the higher fullerenes is that there are simply too many anti-IPR isomers to study exhaustively: It is reported that there are as many as 8149 anti-IPR isomers for C_{70}.[17] However, it is likely that many of the *stable* anti-IPR isomers can be reached from IPR isomers in one pyracylene rearrangement step. We tested this premise by systematically applying our net-based rearrangement to each of the pyracylene unit only once in every IPR isomer up to C_{100}.

As shown in Table 2 under the heading *ratio*, the one-step rearrangements produce two to three times more anti-IPR structures than the IPR isomers. These anti-IPR structures have been subjected to MM3 geometry-optimization[18] and the calculated heats of formation of the most stable structures for each C_n are listed in Table 3. The best anti-IPR isomers are only 9—20 kcal mol^{-1} less stable than the best IPR isomers hav-

Table 2. Number of Unique Anti-IPR Isomers (I) Obtained by One-Step Pyracylene Rearrangement on IPR Fullerenes C_n (n=60, 70, 76 to 100)

n	I	Ratio[a)]	n	I	Ratio
60	1	1.00	88	150	4.29
70	2	2.00	90	167	3.63
76	6	3.00	92	242	2.81
78	13	2.60	94	461	3.44
80	16	2.23	96	584	3.12
82	31	3.44	98	717	2.77
84	49	2.04	100	917	2.04
86	85	4.47	Total = 3492		Av = 2.71

a) Ratio of anti-IPR to IPR structures.

Table 3. MM3 Heats of Formation of the Most Stable IPR and Anti-IPR Isomers of Fullerenes C_n (kcal mol^{-1})

n	ΔH_f^{IPR}	$\Delta H_f^{anti\text{-}IPR}$	Diff[a)]	Diff/C
60	573.39	596.88[b)]	23.49	0.39
70	639.47	656.30	16.83	0.24
76	683.11	693.87	10.76	0.14
78	692.55	705.05	12.50	0.16
80	706.52	720.12	13.60	0.17
82	713.15	725.13	11.98	0.15
84	718.32	733.59	15.27	0.18
86	737.09	754.19	17.10	0.20
88	748.42	763.03	14.61	0.17
90	757.05	777.22	20.17	0.22
92	773.79	790.10	16.31	0.18
94	782.58	801.16	18.58	0.20
96	789.73	809.54	19.81	0.21
98	809.57	822.37	12.80	0.13
100	818.32	827.11	8.79	0.08

a) Diff=$\Delta H_f^{anti\text{-}IPR} - \Delta H_f^{IPR}$ b) Only this C_{60} isomer contains two pentalene units, while all other best anti-IPR isomers contain only one pentalene unit.

ing the same n.[19] Distribution of the MM3-heats of formation in some of the larger anti-IPR fullerenes are compared with those of the IPR-fullerenes in Fig. 3, which clearly shows that low-energy anti-IPR fullerenes can be more stable than high-energy IPR fullerenes. These results suggest that IPR may not be a rigorous rule, especially at high temperatures and for higher fullerenes. This view is in accord with the known stability of substituted pentalenes. Although the parent pentalene (**1**) is unstable (Chart 1) and has not been isolated, alkylated pentalenes are generally stable crystalline compounds with bond alternation.[20] Mechanistic studies on fullerene formation may have to take the possible role of anti-IPR intermediates into accounts.

Growth of Higher Fullerenes by C_2-Addition

We analyze the growth of fullerene by incorporation

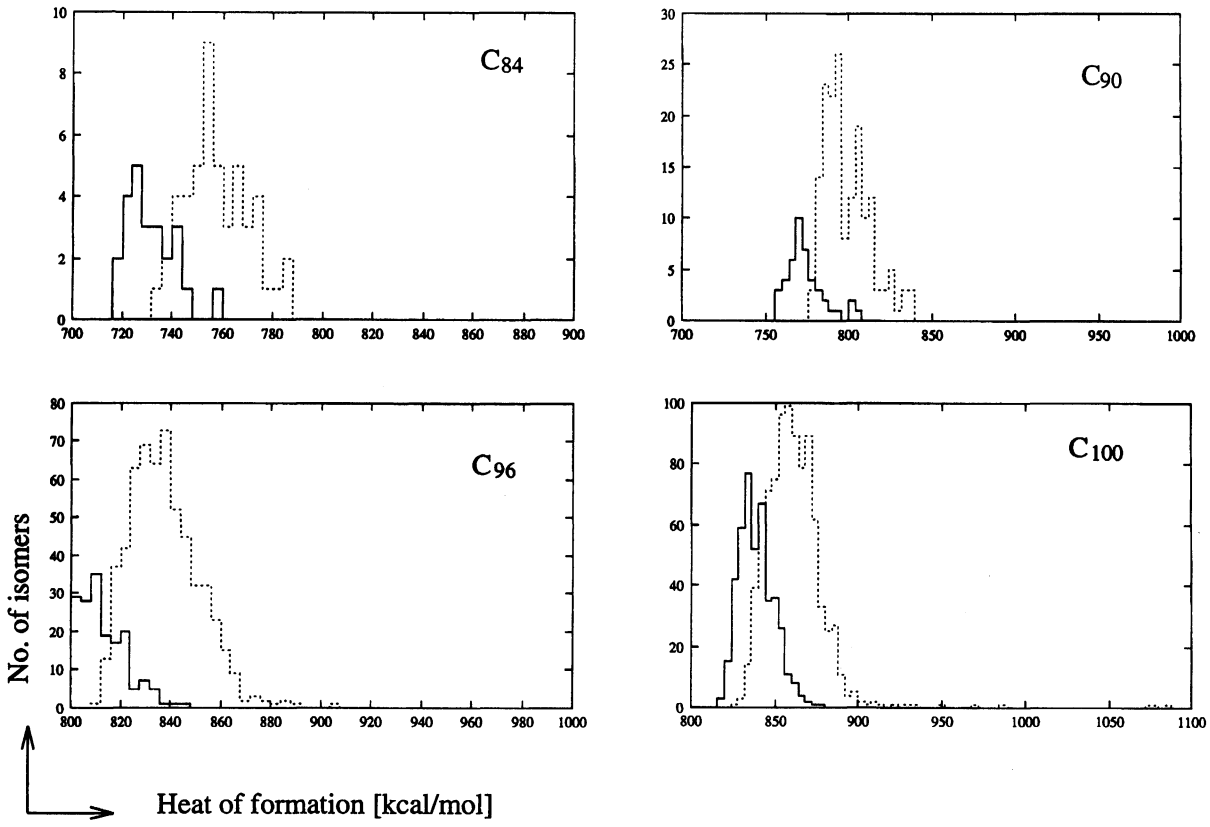

Fig. 3. Distributions of heats of formation (MM3) for all of the IPR (solid line) and stable anti-IPR (dotted line) isomers of C_{84}, C_{90}, C_{96}, and C_{100}.

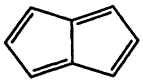

1

Chart 1.

of C_2 clusters.[21] We follow the clever suggestion of Endo and Kroto,[4] namely assume that the reverse of C_2-elimination mechanism (**2**→**3**, Scheme 2), originally proposed by O'Brien et al.[22] to account for the degradation mechanism of fullerenes, should apply to the growth mechanism.[23]

In its broadest sense, the proposed mechanism (**3**→**2**) is the addition of a C_2 fragment onto a hexagonal ring (a Woodward–Hoffmann thermally forbidden 2+2+2+2 cycloaddition). The overall structural change as seen in Scheme 2 is the increase in the number of hexagonal rings by one and the occurrence of a pentalene unit. In view of the modest increase in the energy of anti-IPR fullerene isomers containing only one pentalene unit as mentioned above, such an insertion reaction may well take place under the conditions of fullerene formation. However, unless some mechanism for stabilizing the intermediate **4** is available, its most likely fate will be to lose the C_2 fragment to give back **3** under the reaction condition.

As Endo and Kroto have pointed out,[4] if one of the pentagonal rings in **3** were one 6-ring away as shown in **5** (Scheme 3), a C_2-insertion onto this structure would lead to an intermediate **6**. An extended Stone–Wales (esw) rearrangement[24] in the pyracylene-like partial structure in **6** consisting of two pentagons, one hexagon and a heptagon (thick lines) should lead to a stable hexagon-rich structure **7**, wherein the product of the extended pyracylene rearrangement is indicated with thick lines. **7** is identical with that predicted by Endo and Kroto.[4]

We further assume that, although the C_2-addition must be taking place almost randomly on every hexagonal ring of clusters growing under the reaction conditions, only those having such an esw pathway as given in Scheme 3 would survive. While we have not yet figured out if there are patterns of pentagonal rings suitable for C_2 insertion other than that of **5**, the C_2-growth pathways involving the this pattern are exhaustively enumerated using the net diagram. The partial structure as shown in Scheme 3 can be represented by a bar connecting the two corners in question, as we did in the treatment of pyracylene rearrangement, except that the bar is longer. The overall change can be likewise described by the rotation and translation of the bar, but in this case the length of bar changes (Fig. 4). Details of adjustments that must be given in the vicinity of C_2-insertion point are illustrated in Fig. 5.

A program C2[12] was written which takes care of all the procedures given above (Figs. 4 and 5) from an input of the triangular coordinates of IPR fullerenes and outputs only the IPR C_2-inserted products. The smallest fullerene which can respond to the Kroto-Endo C_2-insertion mechanism as defined above turned out to be D_2–C_{76}. Table 4 summarizes the results of enumerating C_n→C_{n+2} growth pathways up to C_{98}. It is clear that the number of pathways increases rapidly with n. The only C_2-insertion path available to D_2–C_{76} is located at the base of a cap-triangle D (Fig. 6a), producing D_3–C_{78} (Fig. 6b).[25] As noticed by the marks A to E on cap-

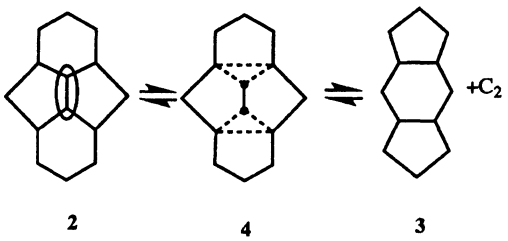

2 4 3

Scheme 2.

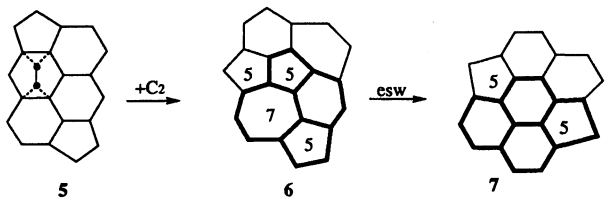

5 6 7

Scheme 3.

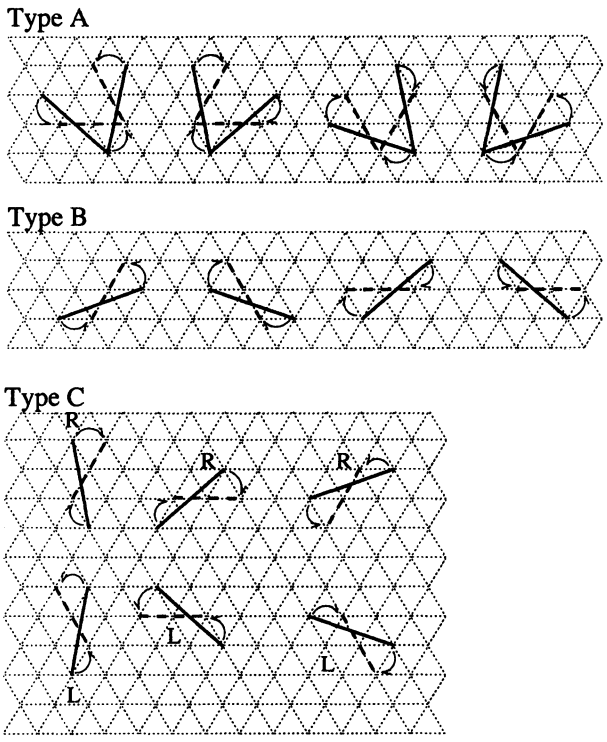

Fig. 4. Graphical representation of the Kroto–Endo C_2-insertion mechanism on a net diagram. Type A=along cap-edge, type B=at the cap-base, type C=across the tubular segment. R and L means the right- and left-side of the unit is adjusted after the rotation-translation of the unit.

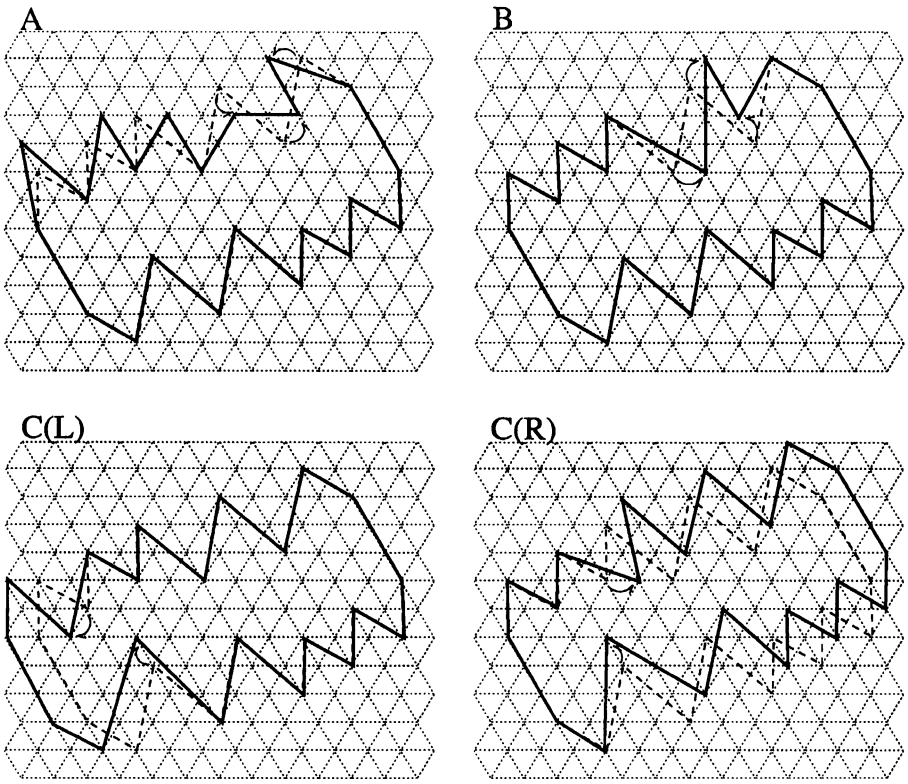

Fig. 5. Changes in the net drawing before (dotted line) and after (solid line) the C_2-insertion reaction according to the Kroto–Endo mechanism. A, B, and C correspond to types A, B, and C, respectively. R and L in type C correspond to the right- and left-side shifts, respectively (see Fig. 4). Type C provides the most complicated case, including six different orientations of the unit. In contrast to pyracylene rearrangement, wherein always the right-side of the rotated-translated unit needs to be shifted, it is necessary here to distinguish two cases, R and L, which signify that either right- or left-side of the unit needs to be adjusted, respectively.

Table 4. Number of C_2-Growth Pathways ($C_n \rightarrow C_{n+2}$), P, in C_{76} to C_{100} Fullerenes by the Kroto–Endo Mechanism

n	P	n	P
76	1	88	48
78	1	90	54
80	3	92	217
82	9	94	351
84	15	96	467
86	31	98	846

Table 5. MM3-Energy and Its Rank among the C_{n+2} Isomers of the Product from C_2-Insertion onto C_n along a Continuous Pathway at the Base of Upper Cap of D_2–C_{76} (see Fig. 6c)

n	$\Delta H_f^{a)}$	Rank[b)]	n	ΔH_f	Rank
76	681.6	1	90	773.8	27
78	695.2	3	92	780.0	9
80	707.0	2	94	785.0	2
82	715.4	3	96	799.6	13
84	744.3[c)]	22—23[d)]	98	814.8	21
86	762.2	13	100	837.0	209
88	767.2	16			

a) MM3-calculated heat of formation, kcal mol^{-1}. b) The stability rank within each IPR C_n isomer family. c) anti-IPR structure. d) The calculated ΔH_f level of this anti-IPR C_{84} structure corresponds to the 22nd to 23rd rank among the 24 IPR isomers of C_{84}.

triangles which have been shifted to the left compared from Fig. 6a, the C_2-insertion is equivalent to the rotation of upper cap. Figure 6c illustrates new positions to which the circled corner would move after further rotation of upper cap, with the number of total carbon atoms of the insertion product given at the end of an arrow. When the cap is rotated almost by one turn to reach C_{84}, pentagons become abutted and an anti-IPR structure appears.

Table 5 lists MM3-energies and the stability ranks of all the products obtained along the continuous C_2-insertion sequence starting from D_2–C_{76}. Clearly, this pathway is likely to discontinue at C_{84} due to the sudden increase in the energy. Program C2 continues the process at the base of upper cap, the product resuming the IPR structure at C_{86}. The increase in energy occurs again at C_{96} after two rotations of cap. The reason for the periodic appearance of such barriers is the strain that arises when the lowered base corner in the upper cap (circled) and the elevated base corner in the lower

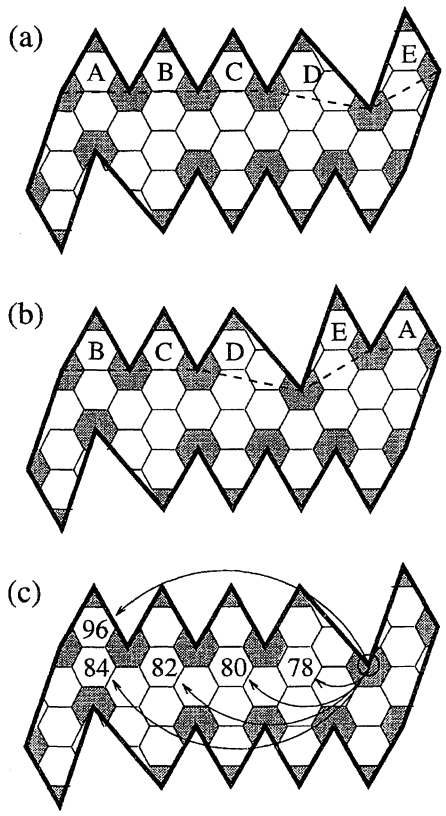

Fig. 6. Net diagrams on a honeycomb lattice. (a) D_2-C_{76}, (b) D_3-C_{78} obtained by C_2-insertion at the base of cap-triangle D of D_2-C_{76}, (c) number of carbon atoms of fullerene (n of C_n) to be obtained by shift of a corner (circled) to the place shown by arrow, drawn on the net diagram of D_2-C_{76}.

cap approach.

The above discussion uses only the insertion pattern of type B (Fig. 4). In order to evaluate the general growth pattern of higher fullerenes, energetically favorable pathways involving all three types are extracted from Table 4 and illustrated in Fig. 7. It is encouraging to find a number of C_2-growth pathways which involve very stable products. A further interesting point to note is that two isomers of C_{84} and an isomer of C_{90} (circled) do not have any possibility of growth as long as we consider only the Kroto–Endo mechanism. In that case, these isomers will tend to accumulate in the reaction mixture. This prediction does not conflict with the observed abundance of C_{84} and C_{90} in the extract of carbon soot from arc-discharge.[16]

Figure 8 is an explosion of the left-half of Fig. 7. The appearance in this Figure of D_2–C_{76}, D_3–C_{78}, C_2–C_{82}, and D_2–C_{84} is in accord with the experimental observations.[16] However, there are contradictions as well: D_{3d}–C_{84} (the fifth in the stability rank) is supposed to accumulate according to our analysis, but has never been observed, and neither C_{2v}–, C'_{2v}–C_{78}, nor C_{2v}–, C_{3v}–C_{82}, which have been experimentally observed, appear in Fig. 8. Further studies on the growth

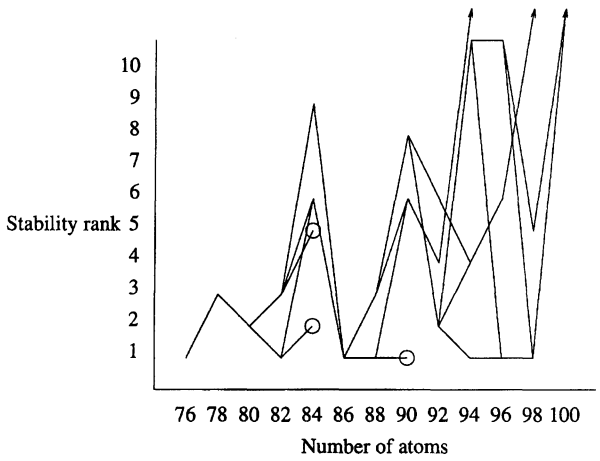

Fig. 7. Energetically favorable pathways of continuous growth of fullerene by C_2-insertion according to the Kroto–Endo mechanism. The stability rank of the product among each IPR C_n isomers is used as the abscissa for clarity of presentation.

mechanism should include a manifold of growth and degradation mechanisms operating under the fullerene formation conditions. For instance, C_2- as well as C_4-insertions leading to anti-IPR intermediates having open structures[21] may have to be taken into account.

Other Applications

1. Leapfrog Operation. The leapfrog operation means multiplication of a fullerene to produce a new structure having three-times more carbon atoms but the same point group symmetry as that of the original fullerene ($C_n \rightarrow C_{3n}$). Fowler[5] has shown that leapfrog fullerenes have closed-shell electronic configurations within the HMO theory. From this rule and the facts that the smallest fullerene is C_{20} and that a C_{22} fullerene cannot be constructed, he gave a general formula C_{60+6k} ($k \neq 1$) for the closed-shell fullerenes.

On the net, the leapfrog operation is equal to multiplying all edge-lengths by $\sqrt{3}$ and rotating by 90° (Fig. 9).[26] This operation becomes a simple arithmetic transformation on an equilateral triangular lattice: The triangular coordinates of corners before the operation (m,n) are related to those after the operation (m',n') by the following equations:[27]

$$m' = m - n, \tag{1}$$

$$n' = m + 2n. \tag{2}$$

Figure 10 illustrates a sample operation.

2. Carbon Cylinder Operation. The carbon cylinder operation provides a convenient method to produce fullerene structures having closed-shell electronic configurations but in this case with nonbonding LUMO.[6] The carbon cylinder operation produces two kinds of cylindrical isomeric series, C_{70+30k} (D_{5h} or D_{5d}) and C_{84+36k} (D_{6h} or D_{6d}), k=0, 1, 2, 3···. Figure 11 illustrates the net diagrams of former series on a

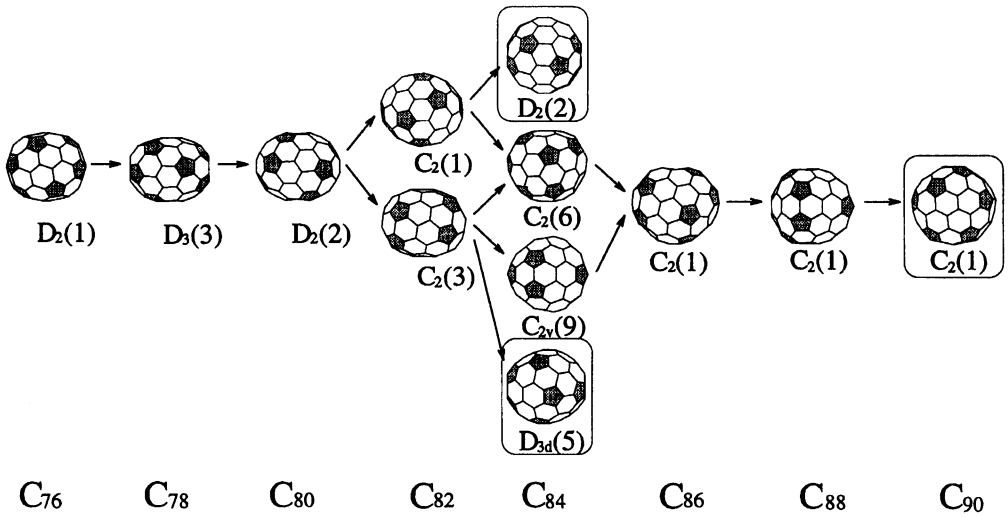

Fig. 8. Energetically favorable pathways of C_2-growth from D_2-C_{76} to C_2-C_{90}. No growth mechanism is available for enclosed structures. Under each perspective drawings are given point group and the stability rank (in parenthesis).

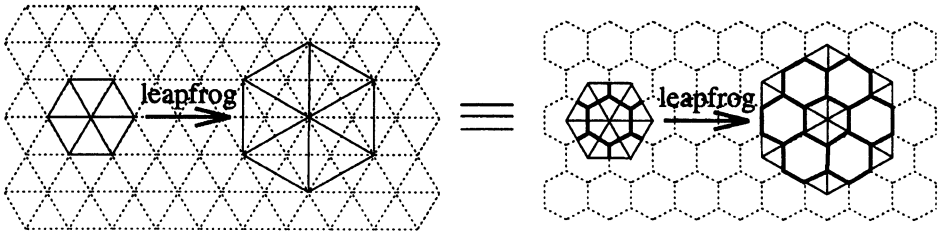

Fig. 9. Leapfrog operation on a network of sp^2-carbon atoms.

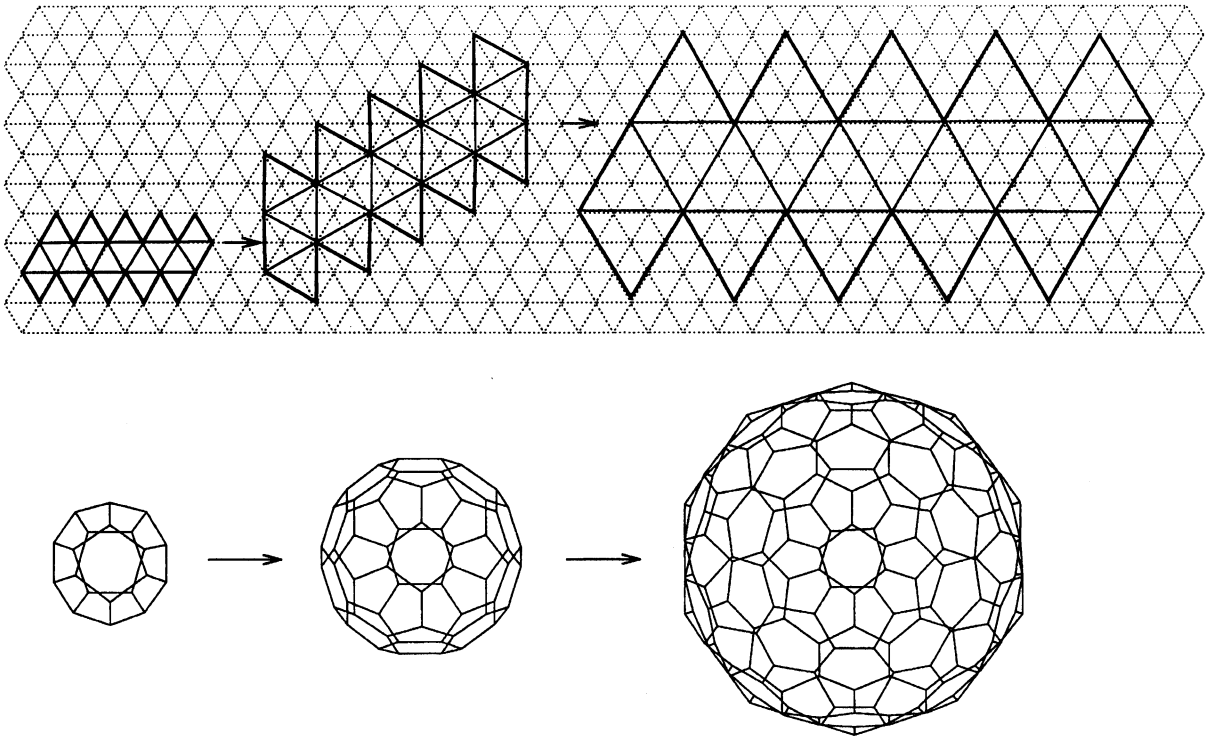

Fig. 10. Examples of leapfrog operation on an equilateral triangular lattice to produce $C_{20}\rightarrow C_{60}\rightarrow C_{180}$.

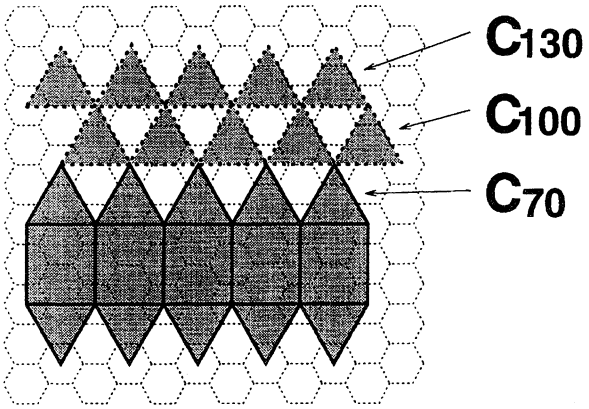

Fig. 11. Net diagram of a carbon cylinder series C_{70+30k} (k=0, 1, 2, 3···). Translation of upper cap as shown corresponds to the carbon cylinder operation.

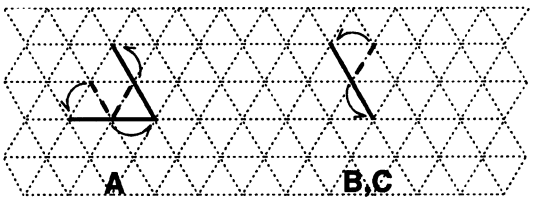

Fig. 12. Graphical representation of C_2-elimination on an equilateral triangular lattice, depending on the environment of pentalene unit in the diagram (see Figs. 1b and 4).

hexagonal lattice, wherein the translation of the upper cap to the dotted lines corresponds to the carbon cylinder operation. A similar illustration can be drawn for the latter series.

3. C_2-Elimination. With all the isomeric anti-IPR structures of C_{20} to C_{60} at hand, it will be a tempting project to exhaustively cover the possibilities of C_2-elimination and study their energetics, in relation to the experimental observations of the C_2-elimination sequence from C_{60} through C_{58}, C_{56}··· to C_{24}.[11,22] The C_2-elimination from a pentalene unit (**2**→**3**, Scheme 2) can be described on a planar lattice as shown in Fig. 12, depending on the three types (A to C) of environments mentioned in Fig. 4.

Conclusions

Manipulation of the skeletal transformations of fullerenes on the formalized net drawings gave the following major conclusions.

(1) It is likely that some of the stable anti-IPR fullerenes are more favorable than some of the unstable IPR isomers. The best anti-IPR isomer of C_{100}, for example, is only 8.8 kcal mol^{-1} less stable than the global energy minimum structure of C_{100}.

(2) The Endo–Kroto C_2-insertion mechanism provides quite a few, energetically favorable growth pathways starting from D_2–C_{76}. There is, however, no plausible path that starts from some stable isomers of C_{84} and C_{90}, suggesting that these isomers tend to accumulate in the reaction mixture.

This work was supported by a Grant-in-Aid for Scientific Research No. 05233107 from the Ministry of Education, Science and Culture.

References

1) M. Yoshida and E. Ōsawa, *Bull. Chem. Soc. Jpn.*, **68**, 2073 (1995).
2) A. Dürer, "Underweysung der Messung," in "The Printed Sources of Western Art," ed by T. Besterman, Collegium Graphicum, Portland, Oregon (1972), Vol. 4.
3) A. J. Stone and D. J. Wales, *Chem. Phys. Lett.*, **128**, 501 (1986).
4) M. Endo and H. W. Kroto, *J. Phys. Chem.*, **96**, 6941 (1992).
5) P. W. Fowler and J. I. Steer, *J. Chem. Soc., Chem. Commun.*, **1987**, 1403.
6) P. W. Fowler, *J. Chem. Soc., Faraday Trans.*, **86**, 2073 (1990).
7) F. Diederich and R. L. Whetten, *Acc. Chem. Res.*, **25**, 119 (1992).
8) F. Diederich, R. L. Whetten, C. Thilgen, R. Ettl, I. Chao, and M. M. Alvarez, *Science*, **254**, 1768 (1991).
9) P. W. Fowler, D. E. Manolopoulos, and R. P. Ryan, *J. Chem. Soc., Chem. Commun.*, **1992**, 408.
10) P. W. Fowler, D. E. Manolopoulos, and R. P. Ryan, *Carbon*, **30**, 1235 (1992).
11) R. L. Murry, D. L. Strout, G. K. Odom, and G. E. Scuseria, *Nature*, **366**, 665 (1993).
12) M. Yoshida and E. Ōsawa, "FULLER, PYRA, and C2," JCPE Program No. P074, obtainable from the Japan Chemistry Program Exchange, Japan Association for International Information, Nakai Bldg., 6-25-4 Honkomagome, Bunkyo-ku, Tokyo 113 (Fax x-81-3-5978-3600).
13) See (Table 3) of Ref. 1.
14) a) C. J. Pope, J. A. Marr, and J. B. Howard, *J. Phys. Chem.*, **97**, 11001 (1993); b) A. L. Lafleur, J. B. Howard, J. A. Marr, and T. Yadav, *J. Phys. Chem.*, **97**, 13539 (1993); c) J. B. Howard, A. L. Lafleur, Y. Makarovsky, S. Mitra, D. J. Pope, and T. K. Yadav, *Carbon*, **30**, 1183 (1992).
15) This remarkable result has been reproduced by other research groups. We thank a referee for this remark.
16) a) K. Kikuchi, N. Nakahara, T. Wakabayashi, M. Honda, H. Matsuyama, T. Moriwaki, S. Suzuki, H. Shiromaru, K. Saito, K. Yamauchi, I. Ikemoto, and Y. Achiba, *Chem. Phys. Lett.*, **188**, 177 (1992); b) K. Kikuchi, N. Nakahara, T. Wakabayashi, S. Suzuki, H. Shiromaru, Y. Miyake, K. Saito, I. Ikemoto, M. Kainosho, and Y. Achiba, *Nature*, **357**, 142 (1992); c) R. Taylor, G. J. Langley, A. G. Avent, T. J. S. Dennis, H. Kroto, and D. R. M. Walton, *J. Chem. Soc., Perkin Trans. 2*, **1993**, 1029; d) R. Taylor, A. G. Avent, P. R. Birkett, T. J. S. Dennis, J. P. Hare, P. B. Hitchcock, J. H. Holloway, E. G. Hope, H. W. Kroto, G. J. Langley, M. F. Meidine, J. P. Parsons, and D. R. M. Walton, *Pure Appl. Chem.*, **65**, 135 (1993); e) H. W. Kroto, K. Prassides, R. Taylor, and D. R. M. Walton, *Phys. Scripta*, **T45**, 314 (1992); f) J. F. Anacleto, R. K. Boyd, S. Pleasance, M. A. Quilliam, J. B. Howard, A. L. Lafleur, and

Y. Makarovsky, *Can. J. Chem.*, **70**, 2558 (1992).

17) D. Babić and N. Trinajstić, *Comput. Chem.*, **17**, 271 (1993).

18) N. L. Allinger, Y. H. Yuh, and J.-H. Lii, *J. Am. Chem. Soc.*, **111**, 8551 (1989).

19) It should be noted that the MM3-energy differences among isomeric fullerenes are much smaller than the MO energy differences (MNDO,[11] STO-3G [R. L. Murry, J. R. Colt, and G. E. Scuseria, *J. Phys. Chem.*, **97**, 4954 (1993)] and higher levels[14]). Although a few available experimental energies compare well with the MM3 results [M. Yoshida and E. Ōsawa, *Fullerene Sci. Technol.*, **1**, 55 (1993)], the large discrepancy between MM and MO energies is still an open question.

20) V. I. Minkin, M. N. Glukhovtsev, and B. Ya. Simkin, "Aromaticity and Antiaromacity," John-Wiley & Sons, New York (1994), pp. 56 and 196.

21) The growth of fullerenes by insertion of larger clusters like C_4 [H. W. Kroto and D. R. M. Walton, in "Carbocyclic Cage Compounds: Chemistry and Applications," ed by E. Ōsawa and O. Yonemitsu, VCH Publishers, New York (1992), Chap. 3] will be the subject of our future studies.

22) S. C. O'Brien, L. R. Heath, R. F. Curl, and R. E. Smalley, *J. Chem. Phys.*, **88**, 220 (1988).

23) Recently Scuseria et al.[11] proposed a new mechanism of C_2-elimination which takes place from a 5/6 bond in a pyracylene unit by way of several intermediates (Chart 2): Since the primary product **A** should quickly rearrange under the severe conditions of fullerene formation to a structure containing only pentagonal and hexagonal rings, it is unlikely that C_2-insertion occurs to the short-lived **A**. Hence we do not consider the reverse of Scuseria's elimination reaction here.

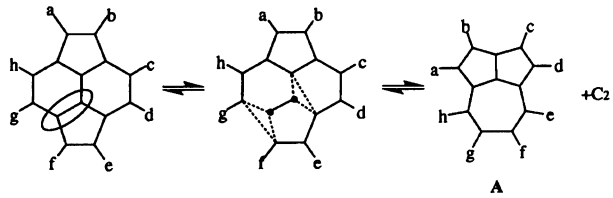

Chart 2.

24) R. Saito, G. Dresselhaus, and M. S. Dresselhaus, *Chem. Phys. Lett.*, **195**, 537 (1992).

25) Note that the honeycomb lattice is used in Fig. 6 (and also Fig. 11) for the illustration purpose.

26) P. W. Fowler, J. E. Cremona, and J. I. Steer, *Theor. Chim. Acta*, **73**, 1 (1988).

27) These equations correspond to the multiplication by $\sqrt{3}$ the rotation by 30°. The fullerene structure thus obtained is identical with that from $\sqrt{3}$-multiplication and 90°-rotation.